

Multi-target-qubit unconventional geometric phase gate in a multi-cavity system

Tong Liu, Xiao-Zhi Cao, Qi-Ping Su, Shao-Jie Xiong & Chui-Ping Yang*

Department of Physics, Hangzhou Normal University, Hangzhou, Zhejiang 310036, China

**e-mail: yangcp@hznu.edu.cn*

Cavity-based large scale quantum information processing (QIP) may involve multiple cavities and require performing various quantum logic operations on qubits distributed in different cavities. Geometric-phase-based quantum computing has drawn much attention recently, which offers advantages against inaccuracies and local fluctuations. In addition, multiqubit gates are particularly appealing and play important roles in QIP. We here present a simple and efficient scheme for realizing a multi-target-qubit unconventional geometric phase gate in a multi-cavity system. This multiqubit phase gate has a common control qubit but different target qubits distributed in different cavities, which can be achieved using a single-step operation. The gate operation time is independent of the number of qubits and only two levels for each qubit are needed. This multiqubit gate is generic, e.g., by performing single-qubit operations, it can be converted into two types of significant multi-target-qubit phase gates useful in QIP and quantum Fourier transform. The proposal is quite general, which can be used to accomplish the same task for a general type of qubits such as atoms, NV centers, quantum dots, and qubits.

Multiqubit gates are particularly appealing and have been considered as an attractive build-

ing block for quantum information processing (QIP). There are two types of significant multiqubit gates, i.e., multiqubit gates with multiple control qubits acting on a single target qubit [1-6], and multiqubit gates with a single qubit simultaneously controlling multiple target qubits [7]. These two kinds of multiqubit gate play important roles in QIP. For instance, a multi-control-qubit gate has applications in quantum algorithms [8,9], error correction [10,11], and quantum Fourier transform [12]; and a multi-target-qubit gate is useful in quantum cloning [13], quantum algorithms [8,12,14], entanglement preparation [15], and error correction [16].

A multiqubit gate can in principle be constructed by using single-qubit and two-qubit basic gates. However, when using the conventional gate-decomposition protocols to construct a multiqubit gate [17,18], the number of basic gates increases and the procedure usually becomes complicated as the number of qubits increases. Hence, building a multiqubit gate may become very difficult since each basic gate requires turning on and off a given Hamiltonian for a certain period of time, and each additional basic gate adds experimental complications and the possibility of more errors. During the past years, there is much interest in *directly* implementing multiqubit gates. Proposals have been presented for directly realizing both multi-control-qubit gates [1-6] and multi-target-qubit gates [7] in various physical systems. Note that the gate implementation using these previous proposals [1-7] was based on non-geometric dynamical evolution.

In recent years, much attention has been paid to fault tolerant quantum computing, which operates essentially based on geometric phase [19-22]. The geometric phase is determined by the global features of the evolution path, which offers potential advantages against local fluctuations.

A great deal of work has been devoted to construct geometric phase gates, which are usually divided into two categories: conventional geometric phase gates and unconventional geometric phase gates. The former needs to remove the dynamical phase by choosing the cyclic evolution in dark states [23] or employing multi-loop schemes (the evolution is driven by a Hamiltonian along several closed loops) [24,25]. But the latter does not require performing *additional* operations to cancel the dynamical phase, because the total phase is dependent only on global geometric features and independent of initial states of the system [26,27]. The unconventional geometric phase gate was first proposed in [26]. According to [26], an unconventional geometric phase gate is characterized by a unitary operator $U(\{\gamma\})$, where γ is the total phase, which consists of a geometric phase and a dynamic phase (see [26]).

During the past years, proposals for realizing both conventional geometric phase gates [23-25,28-31] and unconventional geometric phase gates [26,27,32] were presented. Moreover, high fidelity conventional geometric phase gates have been experimentally demonstrated using NMR [33], superconducting qubits [34], and nitrogen-vacancy (NV) centers [35,36]. In addition, a two-qubit unconventional geometric phase gate has been experimentally realized in a trapped ion system [37]. However, previous works are mainly focused on how to construct single-qubit or two-qubit conventional/unconventional geometric phase gates [23-37], or implementing a multi-control-qubit gate [1-6] and a multi-target-qubit gate [7] based on non-geometric dynamical evolution.

In this work, we consider how to implement a multi-target-qubit unconventional geometric

phase gate, which is described by the following transformation:

$$\begin{aligned} |+\rangle_A \prod_{j=1}^n |i_j\rangle &\rightarrow |+\rangle_A \prod_{j=1}^n e^{i\theta_j \langle +|i_j\rangle} |i_j\rangle, \\ |-\rangle_A \prod_{j=1}^n |i_j\rangle &\rightarrow |-\rangle_A \prod_{j=1}^n e^{i\theta_j \langle -|i_j\rangle} |i_j\rangle, \end{aligned} \quad (1)$$

where subscript A represents a control qubit, subscripts $(1, 2, \dots, n)$ represent n target qubits $(1, 2, \dots, n)$, and $\prod_{j=1}^n |i_j\rangle$ (with $i_j \in \{+, -\}$) is the n -target-qubit computational basis state. For n target qubits, there are a total number of 2^n computational basis states, which form a set of complete orthogonal bases in a 2^n -dimensional Hilbert space of the n qubits. Equation (1) shows that when the control qubit A is in the state $|+\rangle$ ($|-\rangle$), a phase shift $e^{i\theta_j}$ happens to the state $|+\rangle$ ($|-\rangle$) but nothing happens to the state $|-\rangle$ ($|+\rangle$) of the target qubit j ($j = 1, 2, \dots, n$). For instance, under the transformation (1), one has: (i) the state transformation described by following Eq. (18) for a two-qubit phase gate on control qubit A and target qubit j , and (ii) the state transformation described by Eq. (21) below for a three-qubit phase gate on control qubit A and two target qubits $(1, 2)$. Note that the multiqubit phase gate described by Eq. (1) is equivalent to such n two-qubit phase gates, i.e., each of them has a common control qubit A but a different target qubit $1, 2, \dots$, or n , and the two-qubit phase gate acting on the control qubit A and the target qubit j ($j = 1, 2, \dots, n$) is described by Eq. (18).

The multiqubit gate described by Eq. (1) is generic. For example, by performing a single-qubit operation such that $|+\rangle_A \rightarrow \prod_{j=1}^n e^{-i\theta_j} |+\rangle_A$ and $|-\rangle_j \rightarrow e^{i\theta_j} |-\rangle_j$ but nothing to $|-\rangle_A$ and $|+\rangle_j$, the transformation (1) becomes

$$|+\rangle_A \prod_{j=1}^n |i_j\rangle \rightarrow |+\rangle_A \prod_{j=1}^n |i_j\rangle,$$

$$|-\rangle_A \prod_{j=1}^n |i_j\rangle \rightarrow |-\rangle_A \prod_{j=1}^n e^{i2\theta_j \langle -|i_j\rangle} |i_j\rangle, \quad (2)$$

which implies that when and only when the control qubit A is in the state $|-\rangle$, a phase shift $e^{i2\theta_j}$ happens to the state $|-\rangle$ of the target qubit j but nothing otherwise (Fig. 2). For $\theta_j = \pi/2$, the state transformation (2) corresponds to a multi-target-qubit phase gate, i.e., if and only if the control qubit A is in the state $|-\rangle$, a phase flip from the sign $+$ to $-$ occurs to the state $|-\rangle$ of each target qubit. Such a multiqubit phase gate has many applications in QIP [13-16]. In addition, for $\theta_j = \pi/2^j$, the state transformation (2) corresponds to a multi-target-qubit phase gate, i.e., if and only if the control qubit A is in the state $|-\rangle$, a phase shift $\theta_j = \pi/2^j$ happens to the state $|-\rangle$ of each target qubit. It is noted that this multi-target-qubit gate is equivalent to a multiqubit gate with different control qubits acting on the same target qubit (Fig. 3), which is a key element in quantum Fourier transform [8,12].

In what follows, our goal is to propose a simple method for implementing a generic unconventional geometric (UG) multi-target-qubit gate described by Eq. (1), with one qubit (qubit A) simultaneously controlling n target qubits $(1, 2, \dots, n)$ distributed in n cavities $(1, 2, \dots, n)$. We believe that this work is also of interest from the following point of view. Large-scale QIP usually involves a number of qubits. Placing many qubits in a single cavity may cause some fundamental problems such as introducing the unwanted qubit-qubit interaction, increasing the cavity decay, and decreasing the qubit-cavity coupling strength. In this sense, large-scale QIP may need to place qubits in multiple cavities and thus require performing various quantum logic operations on qubits distributed in different cavities. Hence, it is important and imperative to explore how to realize

multiqubit gates performed on qubits that are spatially-separated and distributed in different cavities.

As shown below, this proposal has the following features and advantages: (i) The gate operation time is independent of the number of qubits; (ii) The proposed multi-target-qubit UG phase gate can be implemented using a single-step operation; (iii) Only two levels are needed for each qubit, i.e., no auxiliary levels are used for the state coherent manipulation; (iv) The proposal is quite general and can be applied to accomplish the same task with a general types of qubits such as atoms, superconducting qubits, quantum dots, and NV centers. To the best of our knowledge, this proposal is the first one to demonstrate that a multi-target-qubit UG phase gate described by (1) can be achieved with one qubit simultaneously controlling n target qubits distributed in n cavities.

In this work we will also discuss possible experimental implementation of our proposal and numerically calculate the operational fidelity for a three-qubit gate, by using a setup of two superconducting transmission line resonators each hosting a transmon qubit and coupled to a coupler transmon qubit. Our numerical simulation shows that highly-fidelity implementation of a three-qubit (i.e., two-target-qubit) UG phase gate by using this proposal is feasible with present-day circuit QED technique.

Results

Model and Hamiltonian. Consider a system consisting of n cavities each hosting a qubit and coupled to a common qubit A [Fig. 1(a)]. The coupling and decoupling of each qubit from its

cavity can be achieved by prior adjustment of the qubit level spacings. For instance, the level spacings of superconducting qubits can be rapidly adjusted by varying external control parameters (e.g., magnetic flux applied to the superconducting loop of a superconducting phase, transmon, Xmon or flux qubit; see, e.g., [38-41]); the level spacings of NV centers can be readily adjusted by changing the external magnetic field applied along the crystalline axis of each NV center [42,43]; and the level spacings of atoms/quantum dots can be adjusted by changing the voltage on the electrodes around each atom/quantum dot [44]. The two levels of coupler qubit A are denoted as $|g\rangle_A$ and $|e\rangle_A$ while those of intracavity qubit j as $|g\rangle_j$ and $|e\rangle_j$ ($j = 1, 2, \dots, n$). Applying a classical pulse to qubit A and a classical pulse to each intracavity qubit j [Fig. 1(b),(c)]. For identical qubits, we have $\omega = \omega_{eg_A} = \omega_{eg_j}$, where ω is the pulse frequency and ω_{eg_A} (ω_{eg_j}) is the $|g\rangle \leftrightarrow |e\rangle$ transition frequency of qubit A (qubit j). The system Hamiltonian in the interaction picture reads (in units of $\hbar = 1$)

$$\begin{aligned}
H_I &= \sum_{j=1}^n g_j (e^{-i\delta_j t} a_j^\dagger \sigma_j^- + h.c.) + \sum_{j=1}^n g_{A_j} (e^{-i\delta_{A_j} t} a_j^\dagger \sigma_A^- + h.c.) \\
&+ \sum_{j=1}^n \Omega (\sigma_j^+ + \sigma_j^-) + \Omega (\sigma_A^+ + \sigma_A^-), \tag{3}
\end{aligned}$$

where a_j^\dagger is the photon creation operator for the mode of cavity j , σ_A^+ (σ_j^+) = $|e\rangle_A \langle g|$ ($|e\rangle_j \langle g|$) and σ_A^- (σ_j^-) = $|g\rangle_A \langle e|$ ($|g\rangle_j \langle e|$) are the raising and lowering operators for qubit A (qubit j), $\delta_j = \omega_{eg_j} - \omega_{c_j}$ and $\delta_{A_j} = \omega_{eg_A} - \omega_{c_j}$ are detunings (with ω_{c_j} being the frequency of cavity j), Ω is the Rabi frequency of the pulse applied to each qubit, g_{A_j} (g_j) is the coupling constant of qubit A (j) with cavity j . We choose $|\pm\rangle_j = (|e\rangle_j \pm |g\rangle_j)/\sqrt{2}$ and $|\pm\rangle_A = (|e\rangle_A \pm |g\rangle_A)/\sqrt{2}$ as the rotated basis states of qubit j and qubit A , respectively.

In a rotated basis $\{|+\rangle_l, |-\rangle_l\}$, one has $\sigma_l^+ = (\tilde{\sigma}_{z_l} - \tilde{\sigma}_l^+ + \tilde{\sigma}_l^-) / 2$ and $\sigma_l^- = (\tilde{\sigma}_{z_l} + \tilde{\sigma}_l^+ - \tilde{\sigma}_l^-) / 2$, where $\tilde{\sigma}_{z_l} = |+\rangle_l\langle+| - |-\rangle_l\langle-|$, $\tilde{\sigma}_l^+ = |+\rangle_l\langle-|$, and $\tilde{\sigma}_l^- = |-\rangle_l\langle+|$. Here, $l = 1, 2, 3, \dots, n, A$.

Hence, the Hamiltonian (3) can be expressed as

$$\begin{aligned}
H_I &= \sum_{j=1}^n \frac{1}{2} g_j [e^{-i\delta_j t} a_j^\dagger (\tilde{\sigma}_{z_j} + \tilde{\sigma}_j^+ - \tilde{\sigma}_j^-) + h.c.] \\
&+ \sum_{j=1}^n \frac{1}{2} g_{A_j} [e^{-i\delta_{A_j} t} a_j^\dagger (\tilde{\sigma}_{z_A} + \tilde{\sigma}_A^+ - \tilde{\sigma}_A^-) + h.c.] \\
&+ \sum_{j=1}^n \Omega \tilde{\sigma}_{z_j} + \Omega \tilde{\sigma}_{z_A}. \tag{4}
\end{aligned}$$

In a new interaction picture under the Hamiltonian $H'_0 = \sum_{j=1}^n \Omega \tilde{\sigma}_{z_j} + \Omega \tilde{\sigma}_{z_A}$, one obtains from Eq. (4)

$$\begin{aligned}
H'_I &= \sum_{j=1}^n \frac{1}{2} g_j [e^{-i\delta_j t} a_j^\dagger (\tilde{\sigma}_{z_j} + e^{2i\Omega t} \tilde{\sigma}_j^+ - e^{-2i\Omega t} \tilde{\sigma}_j^-) + h.c.] \\
&+ \sum_{j=1}^n \frac{1}{2} g_{A_j} [e^{-i\delta_{A_j} t} a_j^\dagger (\tilde{\sigma}_{z_A} + e^{2i\Omega t} \tilde{\sigma}_A^+ - e^{-2i\Omega t} \tilde{\sigma}_A^-) + h.c.]. \tag{5}
\end{aligned}$$

In the strong driving regime $2\Omega \gg \{g_j, |\delta_j|, g_{A_j}, |\delta_{A_j}|\}$, one can apply a rotating-wave approximation and eliminate the terms that oscillate with high frequencies. Thus, the Hamiltonian (5) becomes

$$H'_I = \sum_{j=1}^n \frac{1}{2} g_j \tilde{\sigma}_{z_j} (e^{-i\delta_j t} a_j^\dagger + h.c.) + \sum_{j=1}^n \frac{1}{2} g_{A_j} \tilde{\sigma}_{z_A} (e^{-i\delta_{A_j} t} a_j^\dagger + h.c.). \tag{6}$$

For simplicity, we set

$$g_{A_j} = g_j, \quad \delta_j = \delta_{A_j}. \tag{7}$$

The first term of condition (7) can be achieved by adjusting the position of qubit j in cavity j , and second term can be met for identical qubits. Thus, the Hamiltonian (6) changes to

$$H_{eff} = \sum_{j=1}^n H_{eff,j} \tag{8}$$

with

$$H_{eff,j} = \frac{1}{2}g_j(e^{-i\delta_j t}a_j^\dagger + e^{i\delta_j t}a_j)(\tilde{\sigma}_{z_j} + \tilde{\sigma}_{z_A}), \quad (9)$$

where $H_{eff,j}$ is the effective Hamiltonian of a subsystem, which consists of qubit A , intracavity qubit j , and cavity j . In the next section, we first show how to use the Hamiltonian (9) to construct a two-qubit UG phase gate with qubit A controlling the target qubit j . We then discuss how to use the effective Hamiltonian (8) to construct a multi-qubit UG phase gate with qubit A simultaneously controlling n target qubits distributed in n cavities.

Implementing multiqubit UG phase gates. Consider a system consisting of the coupler qubit A and an intracavity qubit j , for which $|\pm\rangle_j$ ($|\pm\rangle_A$) are eigenstates of the operator $\tilde{\sigma}_{z_j}$ ($\tilde{\sigma}_{z_A}$) with eigenvalues ± 1 . In the rotated basis $\{|+\rangle_A|+\rangle_j, |+\rangle_A|-\rangle_j, |-\rangle_A|+\rangle_j, |-\rangle_A|-\rangle_j\}$, the Hamiltonian (9) can be rewritten as

$$H_{eff,j} = g_j(e^{-i\delta_j t}a_j^\dagger + e^{i\delta_j t}a_j) \times \left(|+\rangle_A|+\rangle_j \langle +|_A \langle +|_j - |-\rangle_A|-\rangle_j \langle -|_A \langle -|_j \right), \quad (10)$$

and thus the time evolution operator $U_{Aj}(t)$ corresponding to the Hamiltonian $H_{eff,j}$ can be expressed as

$$\begin{aligned} U_{Aj}(t) &= U_{++ ,j}(t)|+\rangle_A|+\rangle_j \langle +|_A \langle +|_j + |+\rangle_A|-\rangle_j \langle +|_A \langle -|_j \\ &+ |-\rangle_A|+\rangle_j \langle -|_A \langle +|_j + U_{-- ,j}(t)|-\rangle_A|-\rangle_j \langle -|_A \langle -|_j, \end{aligned} \quad (11)$$

where $U_{++ ,j}(t)$ and $U_{-- ,j}(t)$ are given by

$$U_{pp,j}(t) = \hat{T}_j \exp(-i \int_0^t H_{pp,j}(\tau) d\tau)$$

$$\begin{aligned}
&= \hat{T}_j \exp[-ig_j \varepsilon_{pp} \int_0^t (e^{-i\delta_j \tau} a_j^\dagger + e^{i\delta_j \tau} a_j) d\tau] \\
&= \lim_{N \rightarrow \infty} \prod_{n=1}^N \exp[-ig_j \varepsilon_{pp} (e^{-i\delta_j \tau_n} a_j^\dagger + e^{i\delta_j \tau_n} a_j) \Delta\tau] \\
&= \lim_{N \rightarrow \infty} \prod_{n=1}^N D[\Delta\alpha_{pp,j}(\tau_n)] \\
&= D\left(\int_c d\alpha_{pp,j}\right) e^{i\theta_{pp,j}}, \tag{12}
\end{aligned}$$

with

$$H_{pp,j}(t) = \langle p|_A \langle p|_j H_{eff,j} |p\rangle_A |p\rangle_j = g_j \varepsilon_{pp} (e^{-i\delta_j t} a_j^\dagger + e^{i\delta_j t} a_j), \tag{13}$$

where $pp \in \{++, --\}$, $p \in \{+, -\}$, $\varepsilon_{++} = -\varepsilon_{--} = 1$, D is the displacement operator (for details, see Methods below), \hat{T}_j is the time ordering operator and $\Delta\tau = t/N$ is the time interval. From Eq. (12) and Eq. (31) below, one obtains $d\alpha_{pp,j} = -ig_j \varepsilon_{pp} e^{-i\delta_j \tau} d\tau$ and $\theta_{pp,j} = \text{Im}(\int_c \alpha_{pp,j}^* d\alpha_{pp,j})$.

Thus, one has

$$\begin{aligned}
\alpha_{pp,j} &= \int_c d\alpha_{pp,j} = \frac{g_j \varepsilon_{pp,j}}{\delta_j} (e^{-i\delta_j t} - 1), \\
\theta_{pp,j} &= -\frac{g_j^2}{\delta_j} \int_0^{T_j} (1 - \cos \delta_j t) dt, \tag{14}
\end{aligned}$$

where T_j is the evolution time required to complete a closed path.

If $t = T_j$ is equal to $2m_j\pi/|\delta_j|$ with a positive integer m_j , we have $\int_c \alpha_{pp,j} = 0$ according to Eq. (14), which shows that when cavity j is initially in the vacuum state, then cavity j returns to its initial vacuum state after the time evolution completing a closed path. Thus, it follows from Eq. (12) that we have

$$U_{pp,j}(T_j) = D(0) e^{i\theta_{pp,j}} = e^{i\theta_{pp,j}}. \tag{15}$$

Here $\theta_{pp,j}$ is the total phase given by Eq. (14), which is acquired during the time evolution from $t = 0$ to $t = T_j$. Note that $\theta_{pp,j}$ consists of a geometric phase and a dynamical phase.

It follows from Eqs. (11) and (15) that the cyclic evolution is described by

$$\begin{aligned}
U_{Aj}(T_j) &= e^{i\theta_{++j}} |+\rangle_A |+\rangle_j \langle +|_A \langle +|_j + |+\rangle_A |-\rangle_j \langle +|_A \langle -|_j \\
&+ |-\rangle_A |+\rangle_j \langle -|_A \langle +|_j + e^{i\theta_{--j}} |-\rangle_A |-\rangle_j \langle -|_A \langle -|_j.
\end{aligned} \tag{16}$$

Eq. (14) shows that $\theta_{pp,j}$ is independent of index pp . Thus, we have $\theta_{++j} = \theta_{--j} \equiv \theta_j$. Further, according to Eq. (14), after an integration for $T_j = 2m_j\pi/|\delta_j|$ (set above), we have

$$\theta_j = -\frac{g_j^2}{\delta_j} T_j = \frac{2m_j\pi g_j^2}{\delta_j^2}, \tag{17}$$

which can be adjusted by varying the coupling strength g_j and detuning δ_j . Note that a negative detuning $\delta_j < 0$ (see Fig. 1) has applied to the last equality of Eq. (17). The unitary operator (16) describes a two-qubit UG phase gate operation. For $\theta_j \neq 2n\pi$ with an integer n , the phase gate is nontrivial. After returning to the original interaction picture by performing a unitary transformation $U = \exp\{-i(\Omega\tilde{\sigma}_{zj} + \Omega\tilde{\sigma}_{zA})T_j\}$, we obtain the following state transformations: $|+\rangle_A |+\rangle_j \rightarrow e^{i\theta_j} e^{-2i\Omega T_j} |+\rangle_A |+\rangle_j$, $|+\rangle_A |-\rangle_j \rightarrow |+\rangle_A |-\rangle_j$, $|-\rangle_A |+\rangle_j \rightarrow |-\rangle_A |+\rangle_j$, and $|-\rangle_A |-\rangle_j \rightarrow e^{i\theta_j} e^{2i\Omega T_j} |-\rangle_A |-\rangle_j$, which can be further written as

$$\begin{aligned}
|+\rangle_A |+\rangle_j &\rightarrow e^{i\theta_j} |+\rangle_A |+\rangle_j \\
|+\rangle_A |-\rangle_j &\rightarrow |+\rangle_A |-\rangle_j \\
|-\rangle_A |+\rangle_j &\rightarrow |-\rangle_A |+\rangle_j \\
|-\rangle_A |-\rangle_j &\rightarrow e^{i\theta_j} |-\rangle_A |-\rangle_j,
\end{aligned} \tag{18}$$

where we have set $\Omega T_j = k\pi$ (k is a positive integer). For $T_j = 2m_j\pi/|\delta_j|$, we have $2\Omega = k|\delta_j|/m_j$. The result (18) shows that a two-qubit UG phase gate was achieved after a single-step operation described above.

Now we expand the above procedure to a multiqubit case. Consider qubit A and n qubits $(1, 2, \dots, n)$ distributed in n cavities [Fig. 1(a)]. From Eqs. (8) and (9), one can see that: (i) each term of H_{eff} acts on a different intra-cavity qubit but the same coupler qubit A , and (ii) any two terms of H_{eff} , corresponding to different j , commute with each other: $[H_{eff,j}, H_{eff,k}] = 0$ ($j \neq k = 1, 2, \dots, n$). Thus, it is straightforward to show that the cyclic evolution of the cavity-qubit system is described by the following unitary operator

$$U(T) = \prod_{j=1}^n U_{Aj}(T_j), \quad (19)$$

where $U_{Aj}(T_j)$ is the unitary operator given in Eq. (16), which characterizes the cyclic evolution of a two-qubit subsystem (i.e., qubit A and intracavity qubit j) in the rotated basis $|+\rangle_A|+\rangle_j$, $|+\rangle_A|-\rangle_j$, $|-\rangle_A|+\rangle_j$, and $|-\rangle_A|-\rangle_j$.

By changing the detunings δ_j (e.g., via prior design of cavity j with an appropriate frequency), one can have

$$m_1/\delta_1 = m_2/\delta_2 = \dots = m_n/\delta_n, \quad (20)$$

which leads to $T_1 = T_2 = \dots = T_n \equiv T$, i.e., the evolution time for each of qubit pairs $(A, 1)$, $(A, 2)$, \dots , and (A, n) to complete a cyclic evolution is identical. For the setting here, we have $\theta_j = -\frac{g_j^2}{\delta_j}T$ resulting from Eq. (17). Hence, one can easily find from Eqs. (18) and (19) that after a common evolution time T , the n two-qubit UG phase gates characterized by a jointed

unitary operator $U(T)$ of Eq. (19), which have a common control qubit A but different target qubits $(1, 2, \dots, n)$, are simultaneously implemented. As discussed in the introduction, the n two-qubit UG phase gates here are equivalent to a multiqubit UG phase gate described by Eq. (1). Hence, after the above operation, the proposed multiqubit UG phase gate is realized with coupler qubit A (control qubit) simultaneously controlling n target qubits $(1, 2, \dots, n)$ distributed in n cavities.

To see the above more clearly, consider implementing a three-qubit (two-target-qubit) UG phase gate. For three qubits, there are a total number of eight computational basis states, denoted by $\{|+\rangle_A|+\rangle_1|+\rangle_2, |+\rangle_A|+\rangle_1|-\rangle_2, \dots, |-\rangle_A|-\rangle_1|-\rangle_2\}$. According to Eqs. (18) and (19), one can obtain a three-qubit UG phase gate, which is described by

$$\begin{aligned}
|+\rangle_A|+\rangle_1|+\rangle_2 &\rightarrow e^{i(\theta_1+\theta_2)}|+\rangle_A|+\rangle_1|+\rangle_2, & |-\rangle_A|+\rangle_1|+\rangle_2 &\rightarrow |-\rangle_A|+\rangle_1|+\rangle_2, \\
|+\rangle_A|+\rangle_1|-\rangle_2 &\rightarrow e^{i\theta_1}|+\rangle_A|+\rangle_1|-\rangle_2, & |-\rangle_A|+\rangle_1|-\rangle_2 &\rightarrow e^{i\theta_2}|-\rangle_A|+\rangle_1|-\rangle_2, \\
|+\rangle_A|-\rangle_1|+\rangle_2 &\rightarrow e^{i\theta_2}|+\rangle_A|-\rangle_1|+\rangle_2, & |-\rangle_A|-\rangle_1|+\rangle_2 &\rightarrow e^{i\theta_1}|-\rangle_A|-\rangle_1|+\rangle_2, \\
|+\rangle_A|-\rangle_1|-\rangle_2 &\rightarrow |+\rangle_A|-\rangle_1|-\rangle_2, & |-\rangle_A|-\rangle_1|-\rangle_2 &\rightarrow e^{i(\theta_1+\theta_2)}|-\rangle_A|-\rangle_1|-\rangle_2. \quad (21)
\end{aligned}$$

As discussed in the introduction, by applying single-qubit operations, this three-qubit UG phase gate described by Eq. (21) can be converted into a three-qubit phase gate illustrated in Fig. 2 or Fig. 3 for $n = 2$. In the next section, as an example, we will give a discussion on the experimental implementation of this three-qubit UG phase gate for the case of $\theta_1 = \theta_2 = \pi/2$. Based on Eq. (17) and for $T_1 = T_2$ (see above), one can see that the $\theta_1 = \theta_2$ corresponds to $g_1^2/\delta_1 = g_2^2/\delta_2$, which can be met by adjusting g_j (e.g., varying the position of qubit j in cavity j) or detuning δ_j (e.g., prior adjustment of the frequency of cavity j) ($j = 1, 2$).

Possible experimental implementation. Superconducting qubits are important in QIP due to their ready fabrication, controllability, and potential scalability [38,45,46]. Circuit QED is analogue of cavity QED with solid-state devices coupled to a microwave cavity on a chip and is considered as one of the most promising candidates for QIP [45-49]. In above, a general type of qubit, for both of the intracavity qubits and the coupler qubit, is considered. As an example of experimental implementation, let us now consider each qubit as a superconducting transmon qubit and each cavity as a one-dimensional transmission line resonator (TLR). We consider a setup in Fig. 4 for achieving a three-qubit UG phase gate. To be more realistic, we consider a third higher level $|f\rangle$ of each transmon qubit during the entire operation because this level $|f\rangle$ may be excited due to the $|e\rangle \leftrightarrow |f\rangle$ transition induced by the cavity mode(s), which will affect the operation fidelity. From now on, each qubit is renamed “qutrit” since the three levels are considered.

When the intercavity crosstalk coupling and the unwanted $|e\rangle \leftrightarrow |f\rangle$ transition of each qutrit are considered, the Hamiltonian (3) is modified as follows

$$h_I = H_I + \Theta_I, \quad (22)$$

where H_I is the needed interaction Hamiltonian in Eq. (3) for $n = 2$, while Θ_I is the unwanted interaction Hamiltonian, given by

$$\begin{aligned} \Theta_I &= \sum_{j=1}^2 \tilde{g}_j \left(e^{i\tilde{\delta}_j t} a_j \sigma_{fe_j}^+ + h.c. \right) + \sum_{j=1}^2 \tilde{g}_{Aj} \left(e^{i\tilde{\delta}_{Aj} t} a_j \sigma_{fe_A}^+ + h.c. \right) + g_{12} \left(e^{i\Delta t} a_1 a_2^+ + h.c. \right) \\ &+ \sum_{j=1}^2 \tilde{\Omega} \left[e^{i(\omega_{fe_j} - \omega)t} \sigma_{fe_j}^+ + h.c. \right] + \tilde{\Omega} \left[e^{i(\omega_{fe_A} - \omega)t} \sigma_{fe_A}^+ + h.c. \right], \end{aligned} \quad (23)$$

where $\sigma_{fe_j}^+ = |f\rangle_j \langle e|$ and $\sigma_{fe_A}^+ = |f\rangle_A \langle e|$. The first term describes the unwanted off-resonant coupling between cavity j and the $|e\rangle \leftrightarrow |f\rangle$ transition of qutrit j , with coupling constant \tilde{g}_j

and detuning $\tilde{\delta}_j = \omega_{fe_j} - \omega_{c_j}$ [Fig. 5(a,b)], while the second term is the unwanted off-resonant coupling between cavity j and the $|e\rangle \leftrightarrow |f\rangle$ transition of qutrit A , with coupling constant \tilde{g}_{Aj} and detuning $\tilde{\delta}_{Aj} = \omega_{fe_A} - \omega_{c_j}$ [Fig. 5(c)]. The third term of Eq. (23) describes the intercavity crosstalk between the two cavities, where $\Delta = \omega_{c_2} - \omega_{c_1} = \delta_1 - \delta_2$ is the detuning between the two-cavity frequencies and g_{12} is the intercavity coupling strength between the two cavities. The last two terms of Eq. (23) describe unwanted off-resonant couplings between the pulse and the $|e\rangle \leftrightarrow |f\rangle$ transition of each qutrit, where $\tilde{\Omega}$ is the pulse Rabi frequency. Note that the Hamiltonian (23) does not involve $|g\rangle \leftrightarrow |f\rangle$ transition of each qutrit, since this transition is negligible because of $\omega_{c_j}, \omega \ll \omega_{fg_j}, \omega_{fg_A}$ ($j = 1, 2$) (Fig. 5).

When the dissipation and dephasing are included, the dynamics of the lossy system is determined by the following master equation

$$\begin{aligned}
\frac{d\rho}{dt} = & -i [h_I, \rho] + \sum_{j=1}^2 \kappa_j \mathcal{L} [a_j] \\
& + \sum_{l=1,2,A} \{ \Gamma_l \mathcal{L} [\sigma_l^-] + \Gamma_{fe_l} \mathcal{L} [\sigma_{fe_l}^-] + \Gamma_{fg_l} \mathcal{L} [\sigma_{fg_l}^-] \} \\
& + \sum_{l=1,2,A} \{ \Gamma_{l,\varphi f} (\sigma_{ff_l} \rho \sigma_{ff_l} - \sigma_{ff_l} \rho / 2 - \rho \sigma_{ff_l} / 2) \} \\
& + \sum_{l=1,2,A} \{ \Gamma_{l,\varphi e} (\sigma_{ee_l} \rho \sigma_{ee_l} - \sigma_{ee_l} \rho / 2 - \rho \sigma_{ee_l} / 2) \}, \tag{24}
\end{aligned}$$

where $\sigma_{fg_l}^- = |g\rangle_l \langle f|$, $\sigma_{ee_l} = |e\rangle_l \langle e|$, $\sigma_{ff_l} = |f\rangle_l \langle f|$; and $\mathcal{L} [\Lambda] = \Lambda \rho \Lambda^+ - \Lambda^+ \Lambda \rho / 2 - \rho \Lambda^+ \Lambda / 2$, with $\Lambda = a_j, \sigma_l^-, \sigma_{fe_l}^-, \sigma_{fg_l}^-$. Here, κ_j is the photon decay rate of cavity a_j ($j = 1, 2$). In addition, Γ_l is the energy relaxation rate of the level $|e\rangle$ of qutrit l , Γ_{fe_l} (Γ_{fg_l}) is the energy relaxation rate of the level $|f\rangle$ of qutrit l for the decay path $|f\rangle \rightarrow |e\rangle$ ($|g\rangle$), and $\Gamma_{l,\varphi e}$ ($\Gamma_{l,\varphi f}$) is the dephasing rate of the level $|e\rangle$ ($|f\rangle$) of qutrit l ($l = 1, 2, A$).

The fidelity of the operation is given by

$$\mathcal{F} = \sqrt{\langle \psi_{id} | \rho | \psi_{id} \rangle}, \quad (25)$$

where $|\psi_{id}\rangle$ is the output state of an ideal system (i.e., without dissipation, dephasing, and crosstalk considered), while ρ is the final density operator of the system when the operation is performed in a realistic physical system. As an example, we consider that qutrit l is initially in a superposition state $1/\sqrt{2} (|+\rangle_l + |-\rangle_l)$ ($l = 1, 2, A$) and cavity 1 (2) is initially in the vacuum state. In this case, we have $|\psi_{id}\rangle = |\varphi_{id}\rangle \otimes |0\rangle_{c1}|0\rangle_{c2}$, where

$$\begin{aligned} |\varphi_{id}\rangle = & (1/\sqrt{8})(-|+\rangle_A|+\rangle_1|+\rangle_2 + i|+\rangle_A|+\rangle_1|-\rangle_2 + i|+\rangle_A|-\rangle_1|+\rangle_2 + |+\rangle_A|-\rangle_1|-\rangle_2 \\ & + |-\rangle_A|+\rangle_1|+\rangle_2 + i|-\rangle_A|+\rangle_1|-\rangle_2 + i|-\rangle_A|-\rangle_1|+\rangle_2 - |-\rangle_A|-\rangle_1|-\rangle_2), \end{aligned} \quad (26)$$

which is obtained based on Eq. (21) and for $\theta_1 = \theta_2 = \pi/2$.

We now numerically calculate the fidelity of the gate operation. Without loss of generality, consider identical transmon qutrits and cavities. Setting $m_1 = 1$ and $m_2 = 2$, we have $\delta_2 = 2\delta_1$ because of Eq. (20), which corresponds to $g_1/g_2 = 1/\sqrt{2}$ for $\theta_1 = \theta_2$. In order to satisfy the relation $2\Omega \gg |\delta_2|$ and $2\Omega = k|\delta_2|/2$, we set $k = 12$. In addition, we have $\tilde{g}_j \sim \sqrt{2}g_j$, $\tilde{g}_{A_j} \sim \sqrt{2}g_{A_j}$ ($j = 1, 2$), and $\tilde{\Omega} \sim \sqrt{2}\Omega$ for the transmon qutrits [50]. For a transmon qutrit, a ratio 5% of the anharmonicity between the $|g\rangle \leftrightarrow |e\rangle$ transition frequency and the $|e\rangle \leftrightarrow |f\rangle$ transition frequency is readily achieved in experiments. Thus, we set $\tilde{\delta}_j = \delta_j - 0.05\omega_{eg_j}$ and $\tilde{\delta}_{A_j} = \delta_j - 0.05\omega_{eg_{A_j}}$ ($j = 1, 2$). For transmon qutrits, the typical transition frequency between two neighbor levels is between 4 and 10 GHz [51]. Therefore, we choose $\omega_{eg_A}/2\pi, \omega_{eg_j}/2\pi \sim 6.5$ GHz. Other parameters used in the numerical calculation are as follows: $\Gamma_{l,\varphi e}^{-1} = \Gamma_{l,\varphi f}^{-1} = 10.0 \mu\text{s}$,

$$\Gamma_l^{-1} = 30.0 \mu\text{s}, \Gamma_{fe_l}^{-1} = 11.5 \mu\text{s}, \Gamma_{fg_l}^{-1} = 45.0 \mu\text{s} (l = 1, 2, A), \text{ and } \kappa_j^{-1} = 15.0 \mu\text{s} (j = 1, 2).$$

To test how the inter-cavity crosstalk affects the gate fidelity, we plot Fig. 6 for $g_{12} = 0, 0.1g_1, 0.2g_1, 0.3g_1$, which shows the fidelity versus $\delta_1/2\pi$. For simplicity, the dissipation and dephasing of the system are not considered in Fig. 6. As depicted in Fig. 6, the effect of the inter-cavity coupling is negligible as long as $g_{12} \leq 0.1g_1$.

Figure 7 shows the fidelity versus $\delta_1/2\pi$, which is plotted by setting $g_{12} = 0.1g_1$ and now taking the systematic dissipation and dephasing into account. From Fig. 7, one can see that for $\delta_1/2\pi = -3.57$ MHz, a high fidelity 97.0% is achievable for a three-qubit UG phase gate. For $\delta_1/2\pi = -3.57$ MHz, we have $T = T_1 = T_2 = 0.28\mu\text{s}$, $g_1/2\pi = 1.79$ MHz, and $g_2/2\pi = 2.52$ MHz. The values of g_1 and g_2 here are readily available in experiments [52].

The condition $g_{12} \leq 0.1g_1$ is easy to satisfy with the cavity-qutrit capacitive coupling shown in Fig. 4. When the cavities are physically well separated, the inter-cavity crosstalk strength is $g_{12} \sim g_{A_1}C_2/C_\Sigma, g_{A_2}C_1/C_\Sigma$, where $C_\Sigma = C_1 + C_2 + C_q$ (C_q is the qutrit's self-capacitance) [53,54]. For $C_1, C_2 \sim 1$ fF and $C_\Sigma \sim 100$ fF (typical values in experiments), one has $g_{12} = 0.01g_1$. Thus, the condition $g_{12} \leq 0.1g_1$ is readily achievable in experiments.

Energy relaxation time T_1 and dephasing time T_2 of the level $|e\rangle$ can be made to be on the order of $20 - 60 \mu\text{s}$ for state-of-the-art transmon devices [55]. For transmon qutrits, we have the energy relaxation time $T'_1 \sim T_1/2$ and dephasing time $T'_2 \sim T_2$ of the level $|f\rangle$, which are comparable to T_1 and T_2 , respectively. With $\omega_{eg_A}/2\pi, \omega_{eg_j}/2\pi \sim 6.5$ GHz chosen above, we have

$\omega_{c1}/2\pi \sim 6.503$ GHz and $\omega_{c2}/2\pi \sim 6.507$ GHz. For the cavity frequencies here and the values of κ_1^{-1} and κ_2^{-1} used in the numerical calculation, the required quality factors for the two cavities are $Q_1 \sim 6.126 \times 10^5$ and $Q_2 \sim 6.130 \times 10^5$. Note that superconducting coplanar waveguide resonators with a loaded quality factor $Q \sim 10^6$ were experimentally demonstrated [56,57]. We have numerically simulated a three-qubit circuit QED system, which shows that the high-fidelity implementation of a three-qubit UG phase gate is feasible with current circuit QED technique.

Discussion

A simple method has been presented to realize a generic unconventional geometric phase gate of one qubit simultaneously controlling n spatially-separated target qubits in circuit QED. As shown above, the gate operation time is independent of the number n of qubits. In addition, only a single step of operation is needed and it is unnecessary to employ three-level or four-level qubits and not required to eliminate the dynamical phase, therefore the operation is greatly simplified and the experimental difficulty is significantly reduced. Our numerical simulation shows that highly-fidelity implementation of a two-target-qubit unconventional geometric phase gate by using this proposal is feasible with the present circuit QED technique. The proposed multiqubit gate is generic, which, for example, can be converted into two types of important multi-target-qubit phase gates useful in QIP and quantum Fourier transform. This proposal is quite general and can be applied to accomplish the same task with various types of qubits such as atoms, quantum dots, superconducting qubits, and NV centers.

Methods

Geometric phase. Geometric phase is induced due to a displacement operator along an arbitrary path in phase space [58,59]. The displacement operator is expressed as

$$D(\alpha) = e^{\alpha a^\dagger - \alpha^* a}, \quad (27)$$

where a^\dagger and a are the creation and annihilation operators of an harmonic oscillator, respectively.

The displacement operators satisfy

$$D(\alpha_1)D(\alpha_2) = D(\alpha_1 + \alpha_2)e^{iIm(\alpha_1\alpha_2^*)}. \quad (28)$$

For a path consisting of N short straight sections $\Delta\alpha_j$, the total operator is

$$\begin{aligned} D_t &= D(\Delta\alpha_N) \cdots D(\Delta\alpha_j) \\ &= D\left(\sum_{j=1}^N \Delta\alpha_j\right) \exp\left[iIm\left(\sum_{j=2}^N \Delta\alpha_j \sum_{k=1}^{j-1} \Delta\alpha_k^*\right)\right]. \end{aligned} \quad (29)$$

An arbitrary path c can be approached in the limit $N \rightarrow \infty$. Therefore, Eq. (29) can be rewritten as

$$D_t = D\left(\int_c d\alpha\right) e^{i\Theta} \quad (30)$$

with

$$\Theta = Im\left(\int_c \alpha^* d\alpha\right). \quad (31)$$

For a closed path, we have

$$D_t = D(0)e^{i\Theta} = e^{i\Theta}, \quad (32)$$

where Θ is the total phase which consists of a geometric phase and a dynamical phase [22]. In above, equations (27-32) have been adopted for realizing an UG phase gate of one qubit simultaneously controlling n target qubits.

1. Duan, L. M., Wang, B. & Kimble, H. J. Robust quantum gates on neutral atoms with cavity-assisted photon-scattering. *Phys. Rev. A* **72**, 032333 (2005).
2. Wang, X., Sørensen, A. & Mølmeret, K. Multibit gates for quantum computing. *Phys. Rev. Lett.* **86**, 3907 (2001).
3. Zou, X., Dong, Y. & Guo, G. C. Implementing a conditional z gate by a combination of resonant interaction and quantum interference. *Phys. Rev. A* **74**, 032325 (2006).
4. Yang, C. P. & Han, S. n -qubit-controlled phase gate with superconducting quantum-interference devices coupled to a resonator. *Phys. Rev. A* **72**, 032311 (2005); Realization of an n -qubit controlled-U gate with superconducting quantum interference devices or atoms in cavity QED. *ibid.* **73**, 032317 (2006).
5. Monz, T., Kim, K., Hänsel, W., Riebe, M., Villar, A. S., Schindler, P., Chwalla, M., Hennrich, M. & Blatt, R. Realization of the quantum Toffoli gate with trapped ions. *Phys. Rev. Lett.* **102**, 040501 (2009).
6. Jones, C. Composite Toffoli gate with two-round error detection. *Phys. Rev. A* **87**, 052334 (2013).

7. Yang, C. P., Liu, Y. X. & Nori, F. Phase gate of one qubit simultaneously controlling n qubits in a cavity. *Phys. Rev. A* **81**, 062323 (2010); Yang, C. P., Zheng, S. B. & Nori, F. Multiqubit tunable phase gate of one qubit simultaneously controlling n qubits in a cavity. *ibid.* **82**, 062326 (2010); Yang, C. P., Su, Q. P., Zhang, F. Y. & Zheng, S. B. Single-step implementation of a multiple-target-qubit controlled phase gate without need of classical pulses. *Optics Letters* **39**, 11 (2014).
8. Shor, P. W. in *Proceedings of the 35th annual symposium on foundations of computer science*, edited by S. Goldwasser (IEEE Computer Society Press, Los Alamitos, CA, 1994), pp. 124-134.
9. Grover, L. K. Quantum computers can search rapidly by using almost any transformation. *Phys. Rev. Lett.* **80**, 4329 (1998).
10. Shor, P. W. Scheme for reducing decoherence in quantum computer memory. *Phys. Rev. A* **52**, R2493 (1995).
11. Steane, A. M. Error correcting codes in quantum theory. *Phys. Rev. Lett.* **77**, 793 (1996).
12. Nielsen, M. A. & Chuang, I. L. *Quantum computation and quantum information* (Cambridge University Press, Cambridge, 2000).
13. Braunstein, S. L., Bužek, V. & Hillery, M. Quantum-information distributors: quantum network for symmetric and asymmetric cloning in arbitrary dimension and continuous limit. *Phys. Rev. A* **63**, 052313 (2001).

14. Šašura, M. & Bužek, V. Multiparticle entanglement with quantum logic networks: application to cold trapped ions. *Phys. Rev. A* **64**, 012305 (2001).
15. Beth, T. & Rötteler, M. *Quantum Information* (Springer, Berlin, 2001), Vol. 173, Ch. 4, p. 96.
16. Gaitan, F. *Quantum error correction and fault tolerant quantum computing* (CRC Press, USA, 2008).
17. Barenco, A., Bennett, C. H., Cleve, R., DiVincenzo, D. P., Margolus, N., Shor, P., Sleator, T., Smolin, J. A. & Weinfurter, H. Elementary gates for quantum computation. *Phys. Rev. A* **52**, 3457 (1995).
18. Möttönen, M., Vartiainen, J. J., Bergholm, V. & Salomaa, M. M. Quantum circuits for general multiqubit gates. *Phys. Rev. Lett.* **93**, 130502 (2004).
19. Simon, B. Holonomy, the quantum adiabatic theorem, and Berry's phase. *Phys. Rev. Lett.* **51**, 2167 (1983).
20. Berry, M. V. Quantal phase factors accompanying adiabatic changes. *Proc. R. Soc. London, Ser. A* **392**, 45 (1984).
21. Wilczek, F. & Zee, A. Appearance of gauge structure in simple dynamical systems. *Phys. Rev. Lett.* **52**, 2111 (1984).
22. Aharonov, Y. & Anandan, J. Phase Change during a cyclic quantum evolution. *Phys. Rev. Lett.* **58**, 1593 (1987).

23. Duan, L. M., Cirac, J. I. & Zoller, P. Geometric manipulation of trapped ions for quantum computation. *Science* **292**, 1695-1697 (2001).
24. Zhu, S. L. & Wang, Z. D. Implementation of universal quantum gates based on nonadiabatic geometric phases. *Phys. Rev. Lett.* **89**, 097902 (2002).
25. Zhu, S. L. & Wang, Z. D. Universal quantum gates based on a pair of orthogonal cyclic states: Application to NMR systems. *Phys. Rev. A* **67**, 022319 (2003).
26. Zhu, S. L. & Wang, Z. D. Unconventional geometric quantum computation. *Phys. Rev. Lett.* **91**, 187902 (2003).
27. Zheng, S. B. Unconventional geometric quantum phase gates with a cavity QED system. *Phys. Rev. A* **70**, 052320 (2004).
28. Falci, G., Fazio, R., Palma, G. M., Siewert, J. & Vedral, V. Detection of geometric phases in superconducting nanocircuits. *Nature* **407**, 355-358 (2000).
29. Wang, X. B. & Matsumoto, K. Nonadiabatic conditional geometric phase shift with NMR. *Phys. Rev. Lett.* **87**, 097901 (2001).
30. Faoro, L., Siewert, J. & Fazio, R. Non-abelian holonomies, charge pumping, and quantum computation with josephson junctions. *Phys. Rev. Lett.* **90**, 028301 (2003).
31. Solinas, P., Zanardi, P., Zanghì, N. & Rossi, F. Semiconductor-based geometrical quantum gates. *Phys. Rev. B* **67**, 121307 (2003).

32. Feng, X. L., Wang, Z., Wu, C., Kwek, L. C., Lai, C. H. & Oh, C. H. Scheme for unconventional geometric quantum computation in cavity QED. *Phys. Rev. A* **75**, 052312 (2007).
33. Jones, J. A., Vedral, V., Ekert, A. & Castagnoli, G. Geometric quantum computation using nuclear magnetic resonance. *Nature* **403**, 869-871 (2000).
34. Abdumalikov, A. A., Fink, J. M., Juliusson, K., Pechal, M., Berger, S., Wallraff, A. & Filipp, S. Experimental realization of non-Abelian non-adiabatic geometric gates. *Nature* **496**, 482-485 (2013).
35. Arroyo-Camejo, S., Lazariev, A., Hell, S. W. & Balasubramanian, G. Room temperature high-fidelity holonomic single-qubit gate on a solid-state spin. *Nature Comm.* **5**, 4870 (2014).
36. Zu, C., Wang, W. B., He, L., Zhang, W. G., Dai, C. Y., Wang, F. & Duan, L. M. Experimental realization of universal geometric quantum gates with solid-state spins. *Nature* **514**, 72-75 (2014).
37. Leibfried, D., DeMarco, B., Meyer, V., Lucas, D., Barrett, M., Britton, J., Itano, W. M., Jelenković, B., Langer, C., Rosenband, T. & Wineland, D. J. Experimental demonstration of a robust, high-fidelity geometric two ion-qubit phase gate. *Nature* **422**, 412-415 (2003).
38. Clarke, J. & Wilhelm, F. K. Superconducting quantum bits. *Nature* **453**, 1031-1042 (2008).
39. Neeley, M., Ansmann, M., Bialczak, R. C., Hofheinz, M., Katz, N., Erik Lucero, O'Connell, A., Wang, H., Cleland, A. N. & Martinis, John M. Process tomography of quantum memory in a Josephson-phase qubit coupled to a two-level state. *Nat. Physics* **4**, 523-526 (2008).

40. Han, S., Lapointe, J. & Lukens, J. E. *Single-Electron Tunneling and Mesoscopic Devices* (Springer-Verlag press, Berlin Heidelberg, 1991), Vol. 31, pp. 219-222.
41. Barends, R. *et al.* Coherent josephson qubit suitable for scalable quantum integrated circuits. *Phys. Rev. Lett.* **111**, 080502 (2013).
42. Xiang, Z. L., Lü, X. Y., Li, T. F, You, J. Q. & Nori, F. Hybrid quantum circuit consisting of a superconducting flux qubit coupled to a spin ensemble and a transmission-line resonator. *Phys. Rev. B* **87**, 144516 (2013).
43. Neumann, P., Kolesov, R., Jacques, V., Beck, J., Tisler, J., Batalov, A., Rogers, L., Manson, N. B., Balasubramanian, G., Jelezko, F. & Wrachtrup, J. Excited-state spectroscopy of single NV defects in diamond using optically detected magnetic resonance. *New J. Phys.* **11**, 013017 (2009).
44. Pradhan, P., Anantram, M. P.& Wang, K. L. Quantum computation by optically coupled steady atoms/quantum-dots inside a quantum electro-dynamic cavity, arXiv:quantph/0002006.
45. You, J. Q. & Nori, F. Superconducting circuits and quantum information. *Phys. Today* **58**, 42 (2005); You, J. Q. & Nori, F. Atomic physics and quantum optics using superconducting circuits. *Nature* **474**, 589-597 (2011).
46. Buluta, I., Ashhab, S. & Nori, F. Natural and artificial atoms for quantum computation. *Rep. Prog. Phys.* **74**, 104401 (2011); Shevchenkoa, S. N., Ashhabb, S. & Nori, F. Landau-Zener-Stückelberg interferometry. *Phys. Rep.* **492**, 1 (2010); Nation, P. D., Johansson, J. R.,

- Blencowe, M. P. & Nori, F. Stimulating uncertainty: amplifying the quantum vacuum with superconducting circuits. *Rev. Mod. Phys.* **84**, 1 (2012).
47. Blais, A., Huang, R. S., Wallraff, A., Girvin, S. M. & Schoelkopf, R. J. Cavity quantum electrodynamics for superconducting electrical circuits: an architecture for quantum computation. *Phys. Rev. A* **69**, 062360 (2004).
48. Yang, C. P., Chu, S. I. & Han, S. Possible realization of entanglement, logical gates, and quantum-information transfer with superconducting-quantum-interference-device qubits in cavity QED. *Phys. Rev. A* **67**, 042311 (2003).
49. Xiang, Z. L., Ashhab, S., You, J. Q. & Nori, F. Hybrid quantum circuits: superconducting circuits interacting with other quantum systems. *Rev. Mod. Phys.* **85**, 623 (2013).
50. Koch, J., Yu, T. M., Gambetta, J., Houck, A. A., Schuster, D. I., Majer, J., Blais, A., Devoret, M. H., Girvin, S. M. & Schoelkopf, R. J. Charge-insensitive qubit design derived from the Cooper pair box. *Phys. Rev. A* **76**, 042319 (2007).
51. Majer, J. *et al.* Coupling superconducting qubits via a cavity bus. *Nature* **449**, 443-447 (2007); Leek, P. J., Filipp, S., Maurer, P., Baur, M., Bianchetti, R., Fink, J. M., Göppl, M., Steffen, L. & Wallraff, A. Using sideband transitions for two-qubit operations in superconducting circuits. *Phys. Rev. B* **79**, 180511(R) (2009).
52. Fedorov, A., Steffen, L., Baur, M., da Silva, M. P. & Wallraff, A. Implementation of a Toffoli gate with superconducting circuits. *Nature* **481**, 170-172 (2012).

53. Yang, C. P., Su, Q. P. & Han, S. Generation of Greenberger-Horne-Zeilinger entangled states of photons in multiple cavities via a superconducting qutrit or an atom through resonant interaction. *Phys. Rev. A* **86**, 022329 (2012).
54. Su, Q. P., Yang, C. P. & Zheng, S. B. Fast and simple scheme for generating NOON states of photons in circuit QED. *Scientific Reports* **4**, 3898 (2014).
55. Chang, J. B. *et al.* Improved superconducting qubit coherence using titanium nitride. *Appl. Phys. Lett.* **103**, 012602 (2013); Paik, H. *et al.* Observation of high coherence in josephson junction qubits measured in a three-dimensional circuit QED architecture. *Phys. Rev. Lett.* **107**, 240501 (2011); Chow, J. M. *et al.* Implementing a strand of a scalable fault-tolerant quantum computing fabric. *Nature Comm.* **5**, 4015 (2014).
56. Chen, W., Bennett, D. A, Patel, V. & Lukens, J. E Substrate and process dependent losses in superconducting thin film resonators. *Supercond. Sci. Technol.* **21**, 075013 (2008).
57. Leek, P. J., Baur, M., Fink, J. M., Bianchetti, R., Steffen, L., Filipp, S. & Wallraff, A. Cavity quantum electrodynamics with separate photon storage and qubit readout modes. *Phys. Rev. Lett.* **104**, 100504 (2010).
58. Luis, A. Quantum mechanics as a geometric phase: phase-space interferometers. *J. Phys. A: Math. Gen.* **34**, 7677 (2001).
59. Wang, X. & Zarnadi, P. Simulation of many-body interactions by conditional geometric phases. *Phys. Rev. A* **65**, 032327 (2002).

Acknowledgments C. P. Yang was supported in part by the National Natural Science Foundation of China under Grant Nos. 11074062 and 11374083, the Zhejiang Natural Science Foundation under Grant No. LZ13A040002, and the funds from Hangzhou Normal University under Grant Nos. HSQK0081 and PD13002004. This work was also supported by the funds from Hangzhou City for the Hangzhou-City Quantum Information and Quantum Optics Innovation Research Team.

Author contributions T.L and C.P.Y conceived the idea. X.Z.C carried out all calculations under the guidance of Q.P.S and C.P.Y. All the authors discussed the results. T. L and C. P. Y contributed to the writing of the manuscript.

Additional information Competing financial interests: The authors declare no competing financial interests.

Figure 1: (a) Diagram of a coupler qubit A and n cavities each hosting a qubit. A blue square represents a cavity while a green dot labels a qubit placed in each cavity, which can be an atom or a solid-state qubit. The coupler qubit A can be an atom or a quantum dot, and can also be a superconducting qubit capacitively or inductively coupled to each cavity. (b) Cavity j is dispersively coupled to qubit j (placed in cavity j) with coupling constant g_j and detuning $\delta_j < 0$. (c) The coupler qubit A dispersively interacts with cavity j , with coupling constant g_{Aj} and detuning $\delta_{Aj} < 0$ ($j = 1, 2, \dots, n$). Here, $\delta_{Aj} = \delta_j$, which holds for identical qubits A and j .

Figure 2: (a) Schematic circuit of a phase gate with qubit A (a black dot) simultaneously controlling n target qubits (squares). (b) This multiqubit phase gate illustrated in (a) consists of n two-qubit phase gates, each having a shared control qubit (qubit A) but a different target qubit (qubit 1, 2, \dots , or n). Here, the element $2\theta_j$ represents a phase shift $\exp(i2\theta_j)$, which happens to the state $|-\rangle$ of target qubit j ($j = 1, 2, \dots, n$) when and only when the control qubit A is in the state $|-\rangle$ but nothing happens otherwise. For $2\theta_j = \pi$, this gate corresponds to a multi-target-qubit phase gate (useful in QIP [13-16]), i.e., if and only if the control qubit A is in the state $|-\rangle$, a phase flip from the sign $+$ to $-$ occurs to the state $|-\rangle$ of each target qubit.

Figure 3: Schematic circuit of the n successive two-qubit phase gates in quantum Fourier transform. Here, each two-qubit phase gate has a shared target qubit (qubit A) but a different control qubit (qubit 1, 2, \dots , or n). The element $\pi/2^j$ represents a phase shift $\exp(i\pi/2^j)$, which happens to the state $|-\rangle$ of target qubit A if and only if the control qubit j is in the state $|-\rangle$ ($j = 1, 2, \dots, n$). For any two-qubit controlled phase gate described by the transformation $|+\rangle_A|+\rangle_j \rightarrow$

$|+\rangle_A|+\rangle_j$, $|+\rangle_A|-\rangle_j \rightarrow |-\rangle_A|+\rangle_j$, $|-\rangle_A|+\rangle_j \rightarrow |-\rangle_A|+\rangle_j$, and $|-\rangle_A|-\rangle_j \rightarrow e^{i\phi}|-\rangle_A|-\rangle_j$, it is clear that the roles of the two qubits can be interchanged. Namely, the first qubit can be either the control qubit or the target qubit, and the same applies to the second qubit. When the second (first) qubit is a control qubit, while the first (second) qubit is a target, the phase of the state $|-\rangle$ of the first (second) qubit is shifted by $e^{i\phi}$ when the second (first) qubit is in the state $|-\rangle$, while nothing happens otherwise. Thus, the quantum circuit here is equivalent to the circuit illustrated in Fig. 2 for $2\theta_j = \pi/2^j$ ($j = 1, 2, \dots, n$).

Figure 4: Setup of two cavities (1,2) connected by a superconducting transmon qubit A . Here, each cavity represents a one-dimensional coplanar waveguide transmission line resonator, qubit A is capacitively coupled to cavity j via a capacitance C_j ($j = 1, 2$). The two green dots indicate the two transmon qubits (1,2) embedded in the two cavities, respectively. The interaction of qubits (1,2) with their cavities is illustrated in Figs. 5(a) and (b), respectively. The interaction of qubit A with the two cavities is shown in Fig. 5(c). Due to three levels for each qubit considered in our analysis, each qubit is renamed as a qutrit in Fig. 5.

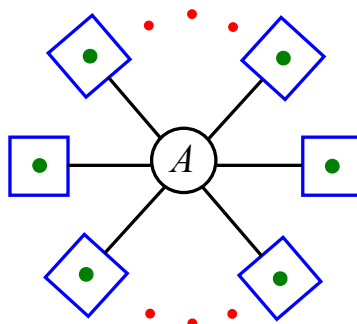
Figure 5: Schematic diagram of qutrit-cavity interaction. (a) Cavity 1 is coupled to the $|g\rangle \leftrightarrow |e\rangle$ transition with coupling strength g_1 and detuning δ_1 , but far-off resonant with the $|e\rangle \leftrightarrow |f\rangle$ transition of qutrit 1 with coupling strength \tilde{g}_1 and detuning $\tilde{\delta}_1$. (b) Cavity 2 is coupled to the $|g\rangle \leftrightarrow |e\rangle$ transition with coupling strength g_2 and detuning δ_2 , but far-off resonant with the $|e\rangle \leftrightarrow |f\rangle$ transition of qutrit 2 with coupling strength \tilde{g}_2 and detuning $\tilde{\delta}_2$. (c) Cavity 1 (2) is coupled to the $|g\rangle \leftrightarrow |e\rangle$ transition of qutrit A with coupling strength g_{A_1} (g_{A_2}) and detuning δ_{A_1}

(δ_{A_2}); but far-off resonant with the $|e\rangle \leftrightarrow |f\rangle$ transition of qutrit A with coupling strength \tilde{g}_{A_1} (\tilde{g}_{A_2}) and detuning $\tilde{\delta}_{A_1}$ ($\tilde{\delta}_{A_2}$). Here, $\delta_j = \omega_{eg_j} - \omega_{c_j}$, $\tilde{\delta}_j = \omega_{fe_j} - \omega_{c_j}$, $\delta_{A_j} = \omega_{eg_A} - \omega_{c_j}$, and $\tilde{\delta}_{A_j} = \omega_{fe_A} - \omega_{c_j}$ ($j = 1, 2$), where ω_{eg_j} (ω_{fe_j}) is the $|g\rangle \leftrightarrow |e\rangle$ ($|e\rangle \leftrightarrow |f\rangle$) transition frequency of qutrit j , ω_{eg_A} (ω_{fe_A}) is the $|g\rangle \leftrightarrow |e\rangle$ ($|e\rangle \leftrightarrow |f\rangle$) transition frequency of qutrit A , and ω_{c_j} is the frequency of cavity j .

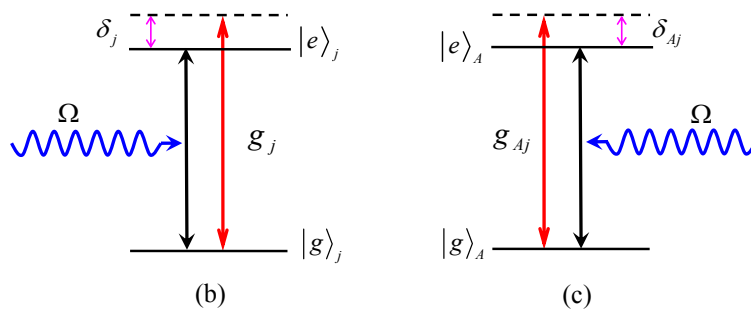
Figure 6: Fidelity versus $\delta_1/2\pi$, plotted for different intercavity coupling strengths but without considering the systematic dissipation and dephasing for simplicity.

Figure 7: Fidelity versus $\delta_1/2\pi$, plotted for $g_{12} = 0$ and $g_{12} = 0.1g_1$ and by taking the systematic dissipation and dephasing into account. The parameters used in the numerical simulation for Figs. 6 and 7 are referred to the text.

[tbp]



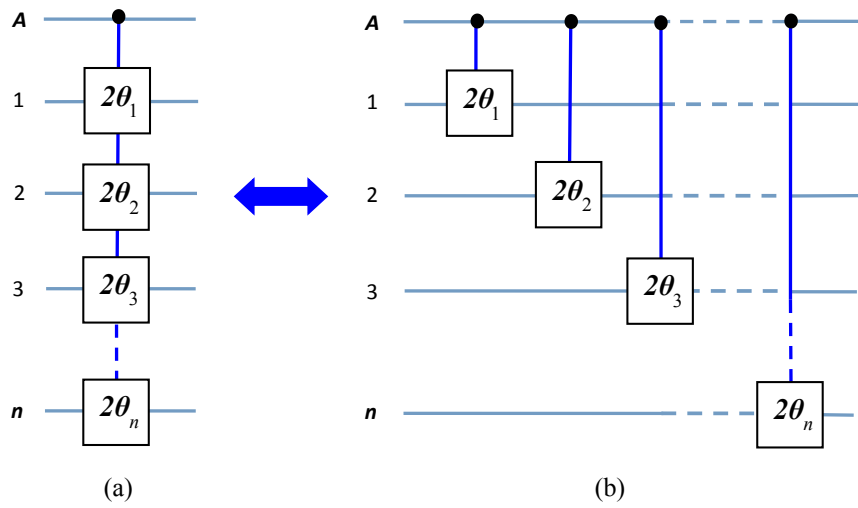
(a)



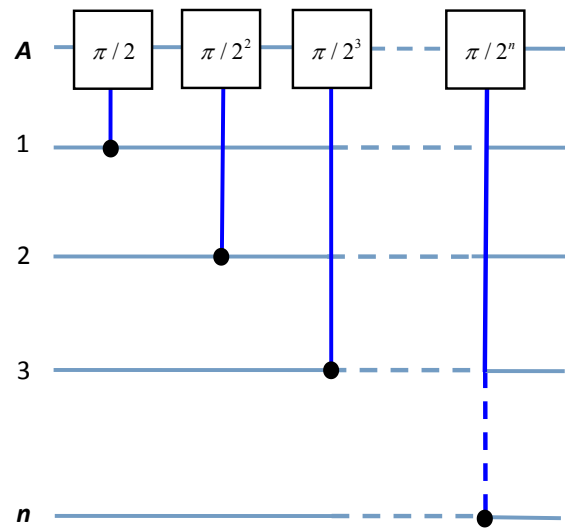
(b)

(c)

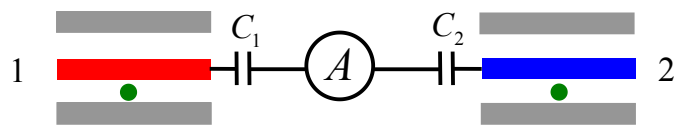
[tbp]



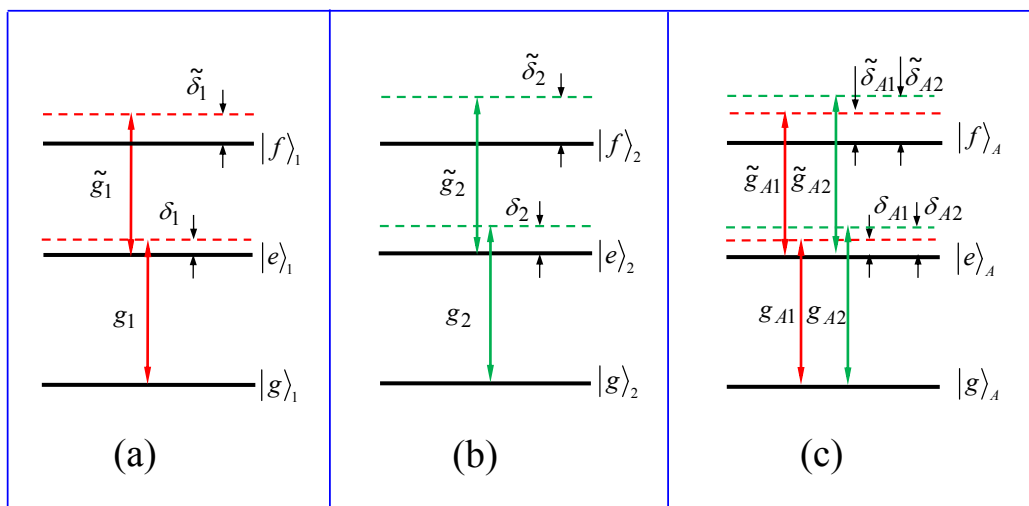
[tbp]



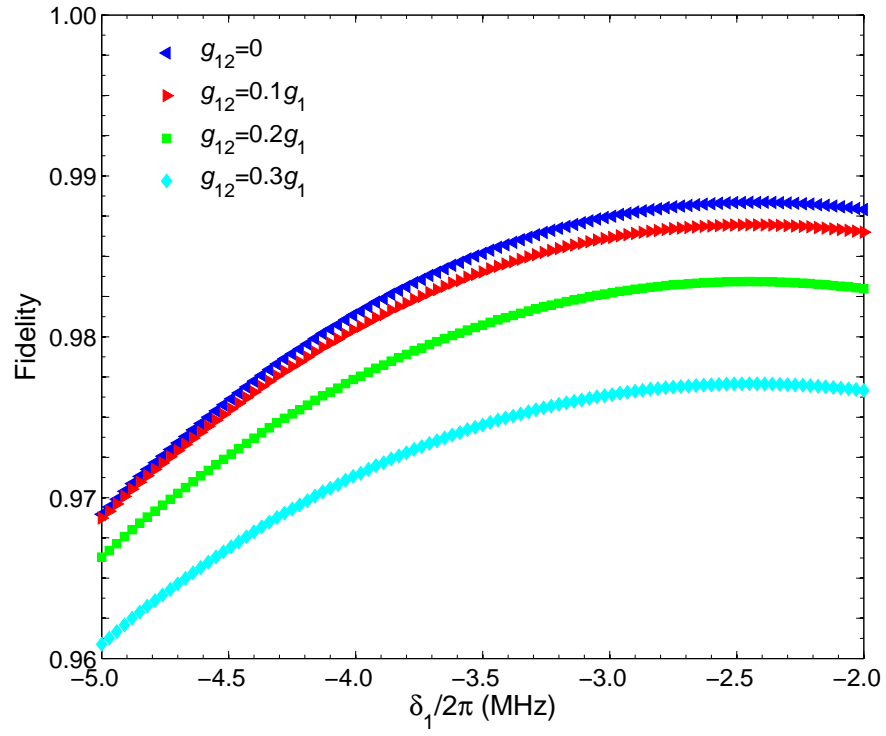
[tbp]



[tbp]



[tbp]



[tbp]

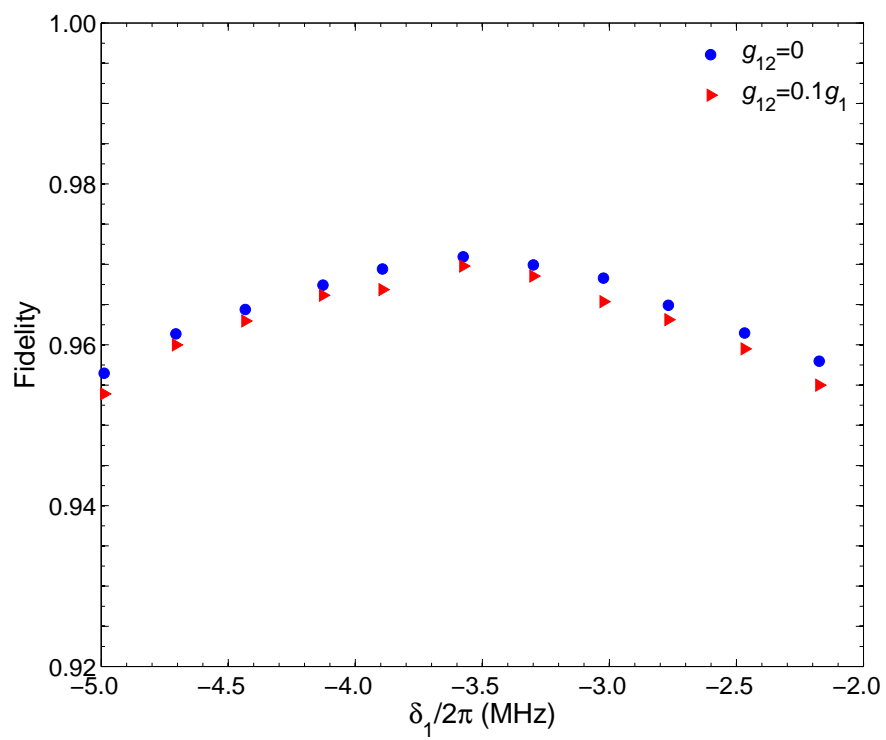


Figure 1

Figure 2

Figure 3

Figure 4

Figure 5

Figure 6

Figure 7